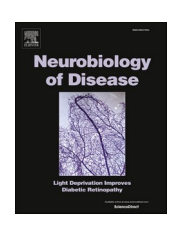
ELSEVIER

Contents lists available at ScienceDirect

### Neurobiology of Disease

journal homepage: www.elsevier.com/locate/ynbdi





# Alpha-synuclein inclusions reduced by PIKfyve inhibition in Parkinson disease cell models

Sara Lucas-Del-Pozo <sup>a,b,1</sup>, Giuseppe Uras <sup>a,b,c,1</sup>, Federico Fierli <sup>a,b</sup>, Veronica Lentini <sup>a,c</sup>, Sofia Koletsi <sup>a,b</sup>, Carlos Lazaro-Hernandez <sup>a,d</sup>, Kai-Yin Chau <sup>a,b</sup>, Derralynn A. Hughes <sup>e</sup>, Anthony H.V. Schapira <sup>a,b,\*</sup>

- a Department of Clinical and Movement Neurosciences, UCL Queen Square Institute of Neurology, London, UK
- b Aligning Science Across Parkinson's (ASAP) Collaborative Research Network, Chevy Chase, MD, USA
- <sup>c</sup> Department of Biomedical Science, University of Sassari, Viale San Pietro, Sassari 07100, Italy
- d Neurology Department, Vall d'Hebron University Hospital, Barcelona, Spain
- <sup>e</sup> Lysosomal Storage Disorders Unit, Royal Free Hospital NHS Foundation Trust and University College London, London, UK

#### ARTICLE INFO

#### Keywords: Parkinson's disease Alpha-synuclein TFEB PIKfyve

#### ABSTRACT

Objective: Parkinson's disease (PD) pathophysiology is associated with a progressive loss of dopaminergic neurons in the substantia nigra and accumulation of insoluble inclusions of misfolded alpha-synuclein. In this study, we used a neuroblastoma-derived cell model overexpressing a pro-aggregation form of alpha-synuclein and human-derived induced-pluripotent stem cells (iPSCs) to investigate the efficacy of PIKfyve-mediated lysosomal biogenesis to reduce alpha-synuclein inclusions.

Methods: We used high-content imaging and enzymatic assays to follow the progression of lysosomal biogenesis, lysosomal catabolism and alpha-synuclein accumulation. The cell models used recapitulated important elements of the biochemical phenotype observed in PD dopaminergic neurons, including alpha-synuclein inclusions and impaired glucocerebrosidase.

Results: PIKfyve inhibition by YM201636 resulted in a lysosomal-dependant reduction of alpha-synuclein inclusions as early as 24 h post-treatment. YM201636 induced an increase in nuclear translocation of TFEB, and an increase in lysosomal markers LAMP1 and HEXA. PIKfyve-inhibition was also tested in neuronal-differentiated neuroblastoma-derived cells and iPSCs-derived dopaminergic neurons. In these cells, YM201636 substantially reduced alpha-synuclein inclusions and increased TFEB nuclear localisation.

Conclusion: These findings suggest that PIKfyve signalling pathways could represent a therapeutic target to reduce alpha-synuclein in PD.

#### 1. Introduction

Parkinson's disease (PD) is the second most common neurodegenerative condition after Alzheimer's disease (AD) (Pringsheim et al., 2014). The main risk factor for developing PD is age, affecting about 3 % of the population from 65 years (Lees, 2010). Histopathologically, PD is defined by the presence of cytoplasmic protein inclusions called Lewy bodies and neurites, whose main component is the protein alphasynuclein (a-synuclein) (Shahmoradian et al., 2019; Spillantini et al., 1997). Both misfolded and hyperphosphorylated a-synuclein at serine129 (pS129) (Fujiwara et al., 2002) along with a lipid-enriched

fraction comprising vesicular structures and dysmorphic organelles (Shahmoradian et al., 2019) are present in these neuronal a-synucleinenriched inclusions. Moreover, other posttranslational modifications of a-synuclein contribute to the spread and amplification of a-synuclein aggregates (Zhang et al., 2023).

Although the aetiology of PD is not fully known, both genetic and environmental factors influence PD susceptibility. Variants of the *GBA1* gene, which encodes the lysosomal enzyme glucocerebrosidase (GCase), when present in bi- or mono-allelic state, constitute the most common genetic risk factor for PD (Gan-Or et al., 2015; Neumann et al., 2009; Sidransky et al., 2009). Up to 1 % of individuals in the general

<sup>\*</sup> Corresponding author at: UCL Queen Square Institute of Neurology, Royal Free Campus, Rowland Hill Street, Hampstead, London NW3 2PF, UK. *E-mail address:* a.schapira@ucl.ac.uk (A.H.V. Schapira).

 $<sup>^{1}</sup>$  Both authors contributed equally as first authors to this article.

population are non-manifesting heterozygous *GBA1* carriers and they have up to a 20-fold increased risk to develop PD as compared to non-carriers (Alcalay et al., 2018; Murugesan et al., 2016; Paciotti et al., 2019; Robak et al., 2017). Additionally, *GBA1* variants are present in 10–15 % of people with PD (Vieira et al., 2024).

Low levels of GCase activity have been reported in PD post-mortem brains without GBA1 variants (Gegg et al., 2012; Mazzulli et al., 2011). Several studies have shown that impaired GCase activity increased asynuclein levels in vitro and in vivo (Cullen et al., 2011; Gegg et al., 2020; Magalhaes et al., 2016; Mazzulli et al., 2011; Yang et al., 2017), linking lysosomal dysfunction to PD pathogenesis. A-synuclein is degraded by the ubiquitin-proteasome system and the autophagy lysosomal pathway (ALP) (Ebrahimi-Fakhari et al., 2011; Wallings et al., 2019). However, excessive a-synuclein accumulation causes lysosomal dysfunction in people with PD-derived induced-pluripotent stem cells (iPSC)-midbrain neurons (Cuddy et al., 2019) and reduces lysosomal catabolism in human midbrain dopaminergic models of synucleinopathies through disrupting GCase trafficking from the endoplasmatic reticulum (ER) to the lysosomes (Henderson et al., 2020; Mazzulli et al., 2016). Additionally, a-synuclein accumulation at the ER has been reported to induce ER fragmentation, compromising its protein-folding capacity and leading to the misfoding and aggregation of lysosomal hydrolases (Stojkovska et al., 2022). These abnormalities of lysosomal metabolism are expected to further exacerbate deficits in a-synuclein turnover. Furthermore, increased a-synuclein levels have been shown to independently reduce GCase activity in the absence of GBA1 variants, intensifying a-synuclein pathology (Mazzulli et al., 2011; Mazzulli et al., 2016). Considering lysosomal dysfunction plays an essential role in the progression of PD, therapeutic strategies aimed potentiating lysosomal synthesis and catabolic efficiency have gained considerable attention.

Transcription Factor EB (TFEB), a member of the MiT/TFE family, is a helix-loop-helix leucine-zipper transcription factor capable of recognising sequences of the Coordinated Lysosomal Expression and Regulation (CLEAR) gene network, widely distributed among lysosomal biogenesis gene promoters, eventually modulating cellular clearance processes (Palmieri et al., 2011). TFEB positively regulates expression of lysosomal biogenesis-related genes, enhancing lysosomal catabolic activity (Sardiello et al., 2009). It promotes autophagy by upregulating autophagosome formation, facilitating autophagosome-lysosome fusion, and stimulating lysosomal exocytosis, thereby supporting the clearance of intracellular misfolded proteins (Medina et al., 2011; Settembre et al., 2011). TFEB is constitutively found in its phosphorylated state in the cytoplasm attached to the lysosome membrane. Upon dephosphorylation of multiple serine residues TFEB re-locates to the nucleus, thus exerting its transcriptional activity (Napolitano et al., 2018). Mechanistic target of rapamycin complex 1 (mTORc-1) regulates TFEB subcellular localisation by phosphorylating serine-211 and promoting TFEB cytoplasmatic retention (Napolitano et al., 2018; Sardiello et al., 2009).

A regulator of TFEB translocation is PIKfyve, a lipid kinase that phosphorylates phosphatidylinositol-3-phosphate (PI(3)P), producing PI(3,5)P2. It is named after its function and domain structure "phosphoinositide kinase for five position containing a FYVE-finger" (Rivero-Rios and Weisman, 2022) and contributes to regulating membrane homeostasis, endosomal trafficking and autophagy (Ikonomov et al., 2019). To execute its kinase activity, PIKfyve has to form a complex including the scaffold protein Vac14 and the lipid phosphatase Fig4. (Rivero-Rios and Weisman, 2022). PIKfyve is crucial to lysosome reformation and generation of early endosomes (Bissig et al., 2019). In mammalian cells, PIKfyve plays roles in the regulation of transcription, as PIKfyve positively regulates mTORc1-dependent phosphorylation of TFEB (Hasegawa et al., 2022). Upon PIKfyve inhibition, Protein Phosphatase-2 A (PP2A) dephosphorylates TFEB, resulting in TFEB nuclear translocation (Hasegawa et al., 2022) and upregulation of the expression of genes for autophagy and lysosomal function (Hasegawa et al., 2022). Additionally, in vitro data suggests that PP2A activity is, to some extent,

partially negatively regulated by PIKfyve, as enhanced dephosphorylation of TFEB by PP2A is observed under PIKfyve inhibition (Hasegawa et al., 2022).

The initial inhibitor identified for PIKfyve was YM201636, a pyrimidine-based kinase inhibitor with good potency against PIKfyve *in vitro* (Hayakawa et al., 2006) and selectivity over several lipid kinase family members (Hayakawa et al., 2006; Ikonomov et al., 2019). PIKfyve-inhibition efficacy as a therapeutic intervention for PD has been highlighted in a genetic screening, in which PIKfyve-knockdown prevented an increase of a-synuclein aggregation (See et al., 2021).

To investigate whether activation of TFEB signalling through PIKfyve-inhibition prevents a-synuclein aggregation, we used a neuro-blastoma cell model overexpressing a mutant form of the *SNCA* gene which leads to a rapid aggregation of a-synuclein following its interaction with lipid-membrane organelles (Imberdis et al., 2019). In this model, the familial PD mutation E46K was "amplified" by introducing two analogous extra-lysine mutations into the nearby KTKEGV-repetitive motive in positions E35K, E46K, and E61K (Dettmer et al., 2015b). The presence of such mutations leads to a fast a-synuclein aggregation, detectable after 24–48 h in culture (Imberdis et al., 2019), since mutations located within the KTKEGV sequence affect the specificity of a-synuclein membrane affinity.

We report that inhibition of PIKfyve using the compound YM201636 results in a reduction of a-synuclein inclusions, is lysosome-dependent and associated with TFEB nuclear translocation. The a-synuclein inclusions' reduction induced by YM201636, was reproduced in both differentiated neuroblastoma cells and in human hiPSC-derived dopaminergic neurons carrying the p.A53T SNCA PD familial mutation.

#### 2. Methods

Extended methods available in the Supplementary Datafile.

#### 2.1. Cell line, cell culture and compound treatment

Wild-type SH-SY5Y were used as parental control (CRL-2266, Atcc, UK). SH-SY5Y constitutively expressing the 3 K-SNCA gene were a gift from Dr. Ulf Dettmer (Harvard, USA). Cells were maintained in DMEM/ F12 (Gibco®) with Glutamax® (Gibco®) supplemented with 10 % fetal bovine serum (Gibco®) and Penicillin/Streptomycin (Gibco®). Cells were passaged to maintain 50–70 % confluency.

Wild-type and *3 K-SNCA* SH-SY5Y were differentiated into neurons using a retinoic acid-based protocol, as previously described (Gegg et al., 2020; Uras et al., 2022). Differentiated cells were in culture for 9 days.

3\*10<sup>4</sup> cells were seeded into each well in 96 well/plates (Phenoplate®). 24 h post-seeding, cells were treated with the appropriate compound or vehicle. Afterwards, cells were incubated for 24 h and subsequently used for downstream analysis. Compounds used were YM201636 (Cayman Chemical, US) and ambroxol hydrochloride (Merck®, London, UK).

iPSCs-derived dopaminergic neurons (Fujifilm Cellular Dynamics, Inc) with a heterozygous gene-edited p.A53T mutation (iCell A53T DOPA) and isogenic controls (iCell DOPA) were differentiated according to manufacturer instructions using iCell Neural Medium Bottle supplemented with 2 % iCell Neural Supplement B and 1 % iCell Nervous system supplement. Cells were seeded at a  $4.5\!\!^{*}10^4/\text{cm}^2$  density. Half media change was performed every 48 h. After 11 days in culture, iCell dopaminergic neurons were treated with 1  $\mu$ M YM201636 for 7 days.

iCell® DopaNeurons PD SNCA A53T HZ (FCDI) neurons are derived from iPSCs and differentiated into midbrain floorplate dopaminergic neurons, with >70 % of the population expressing tyrosine hydroxylase (TH) as indicated by the manufacturer, confirming their dopaminergic identity (https://www.fujifilmcdi.com/icell-dopaneurons-pd-snca-a53t-hz-01279-gdpna53t01279). The A53T mutation in *SNCA* increases a-synuclein's tendency to aggregate, offering a biologically relevant model for studying Parkinson's disease pathology. The isogenic

control line allows for direct comparison to assess the specific impact of the A53T variant.

#### 2.2. Cell staining

Cells were fixed in 4 % paraformaldehyde (Severn-Biotech Ltd.®) and permeabilized with ice-cold methanol, blocked in 5 % normal goat serum (Abcam®) and incubated with primary antibody. Primary antibodies used according to the experiment: monoclonal rabbit antisynuclein 1:750 (Abcam®); monoclonal mouse anti-GBA 1:1000 (Anti-GBA mAb (2E2), Calbiochem®); monoclonal rabbit anti-TFEB 1:500 (Anti-TFEB D207D Rabbit mAb, Cell Signalling®); monoclonal mouse anti-LAMP1 1:1000 (BD® Transduction Lab); monoclonal mouse antisynclein 1:750 (Abcam®). Finally, cells were incubated with secondary antibody. The secondary antibodies used: AlexaFluor 488 1:2000 (Invitrogen®); AlexaFluor 568 1:2000 (Invitrogen®); AlexaFluor 647 1:2000 (Invitrogen®).

For lysosomal studies, LysoTracker® Red DND-99 (Life Technologies®) at 65 nM for 45 min was used following manufacture's recommendations. Following this, the medium was replaced with fresh media containing 20 nM Hoesch33342 (Thermo Fisher®) for five minutes and washed three times with media. Plates were imaged at 50 min using the Opera Phenix® Plus High-Content Screening System (PerkinElmer®).

DQ-red BSA (Thermo Fisher®) was performed as previously described (Marwaha and Sharma, 2017). Briefly, after 23 h treatment with the relevant compound or vehicle, media was removed from each well. Cells were washed once with pre-warmed  $1\times$  PBS. Subsequently, media containing DQ-Red BSA 10 µg/ml and relevant compound was added to each well for 1 h at 37 °C. Then, media was removed, and cells fixed with 4 % paraformaldehyde (Severn-Biotech Ltd.®). Afterwards, cells were incubated for 3 min with DAPI 1µg/ml in 1xPBS solution. Finally, cells were imaged using the Opera Phenix® Plus High-Content Screening System (PerkinElmer®).

#### 2.3. High content imaging

Cell imaging was performed using Opera Phenix® Plus High-Content Screening System (PerkinElmer®). Image acquisition was done using Harmony® high-content imaging and analysis software (PerkinElmer®). Images were acquired in confocal mode, 63× water immersion objective. Each 96-well plate included multiple experimental conditions. Between 3 and 9 replicate wells per condition were included in every plate, depending on the number of experimental conditions. Within each well, 5 to 7 randomly selected fields were imaged using Harmony® High-Content Imaging and Analysis Software (PerkinElmer®), allowing efficient coverage of both the central and peripheral areas of the well. Once the fields were defined in the Harmony® script for an experiment, the same fields were automatically applied to all wells, ensuring consistency across samples and minimising potential operator bias. Quantitative image analysis was performed using the Columbus® Image Data Storage and Analysis System (PerkinElmer®) according to standard protocols. The software automatically calculated the mean intensity or mean number of inclusions per cell for each well by pooling data from all imaged fields. Final well-level results were obtained by aggregating the data across all acquired fields. Detailed image acquisition and analysis protocols are provided in the supplementary materials.

### 2.4. GCase activity assay and Homogeneous Time Resolved Fluorescence aggregated a-synuclein quantification

In vitro GCase activity in cell lysates using a 4-methylumbelliferyl- $\beta$ -D-glucopyranoside-based fluorometric assay was performed. A detailed protocol is available in the supplementary materials.

The Cisbio® Fluorescence Resonance Energy Transfer (FRET) assay (Perkin Elmer®, Cisbio®) was used to quantify aggregated a-synuclein, following the manufacturer's recommendations.

#### 2.5. Quantitative real-time PCR

mRNA was extracted using the RNAeasy-kit (Qiagen®) and cDNA was synthesised using the QuantiTect® Reverse Transcription kit (Qiagen). Gene expression was determined by quantitative real-time polymerase chain reaction (QuantStudio® 1 Real-Time PCR System, Applied Biosystems®) in triplicate wells using TaqMan® Gene Expression Assays (probes used detailed in the supplementary materials). Relative gene-expression was normalised to the corresponding value of GAPDH-expression in each sample and the fold-changes relative to the control values within the same experiment were determined using the  $2\text{-}\Delta\Delta\text{Ct}$  method.

#### 2.6. Experimental design and data analysis

Each biological replicate was defined as one vial of cells. Each independent experiment included one biological replicate and was repeated three times on different days.

Within each 96-well plate, technical replicates were represented by multiple wells per experimental condition. For each well, 5 to 7 microscopic fields were imaged, and the data from all imaged fields were averaged to yield a single value per well. For each condition, between 3 and 9 wells were included per plate, depending on the total number of conditions tested and practical constraints such as plate capacity and reagent availability.

To control for plate-to-plate variability, all data were normalised to the mean of the DMSO control wells within the same plate. Following normalisation, data from technical replicates (wells) were averaged within each plate to obtain a single value per condition per biological replicate. These averaged, normalised values were used for statistical analysis and are represented as individual data points ("dots") in the figures, corresponding to biological replicates. Statistical analysis was performed using the mean normalised value per condition per plate as the unit of analysis.

The pooled normalised data were assessed for normality using the D'Agostino–Pearson test and the Shapiro–Wilk test. Based on the distribution of the data, multiple group comparisons were conducted using one-way ANOVA with Bonferroni correction or Kruskal–Wallis test with Dunn's post-hoc analysis, as appropriate. For pairwise comparisons, either unpaired two-tailed t-tests or Mann–Whitney U tests were applied. Statistical significance was set at p < 0.05.

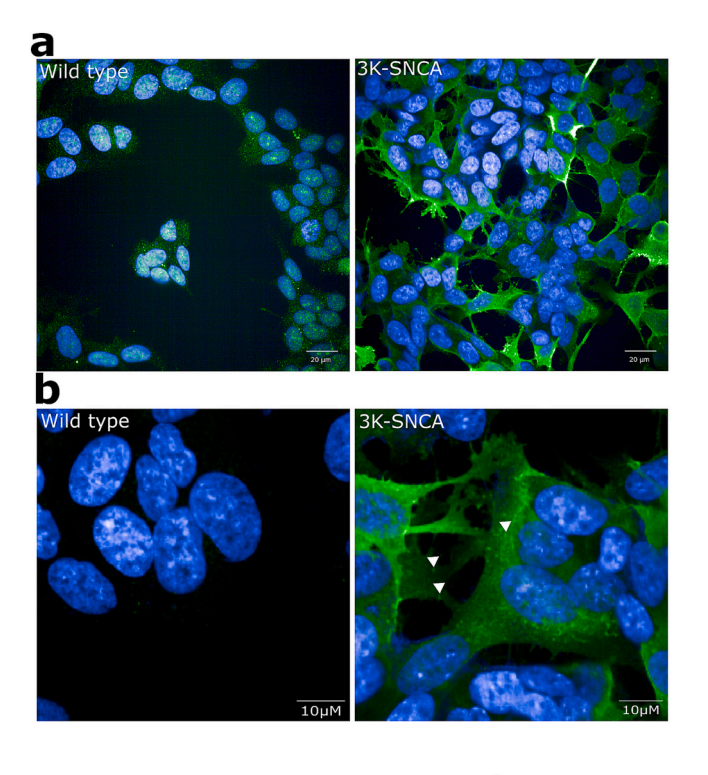
All statistical analyses were performed using GraphPad Prism® version 10.0.2 (GraphPad Software, San Diego, CA, USA).

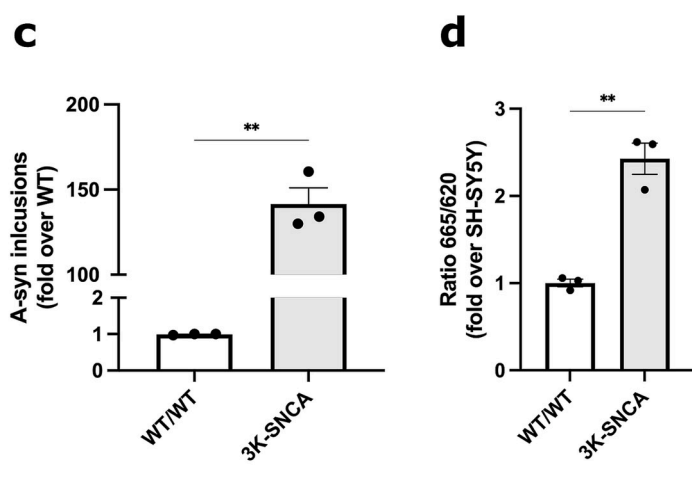
#### 3. Results

## 3.1. Overexpression of 3 K-SNCA gene leads to formation of a-synuclein inclusions and compromises lysosomal hydrolase GCase

To confirm overexpression of *3 K-SNCA* leads to a rapid formation of visible a-synuclein inclusions, we compared the amount of inclusions per cell in *3 K-SNCA* mutant SH-SY5Y to wild-type SH-SY5Y. In wild-type cells, a-synuclein staining was diffuse. In contrast, 3 K-SNCA cells exhibited areas of intense focal accumulation. High-content imaging analysis showed not only an increased mean of a-synuclein signal intensity in the cell body of *3 K-SNCA* cells, likely due to the constitutive overexpression, but also a statistically significant increase in the number of a-synuclein round cytoplasmatic inclusions per cell as early as 24 h post-seeding (Fig. 1; a-c). These results recapitulate the increase in a-synuclein inclusion formation in *3 K-SNCA* cells previously described (Dettmer et al., 2015a; Imberdis et al., 2019). To confirm this, we performed a FRET-HTRF® assay to quantify aggregates. Our results show an increase of the ratio in the *3 K-SNCA* cells (Fig. 1; d), in line with our initial findings.

Subsequently, we investigated whether the presence of inclusions leads to lysosomal dysfunction. We tested GCase (Mazzulli et al., 2011),





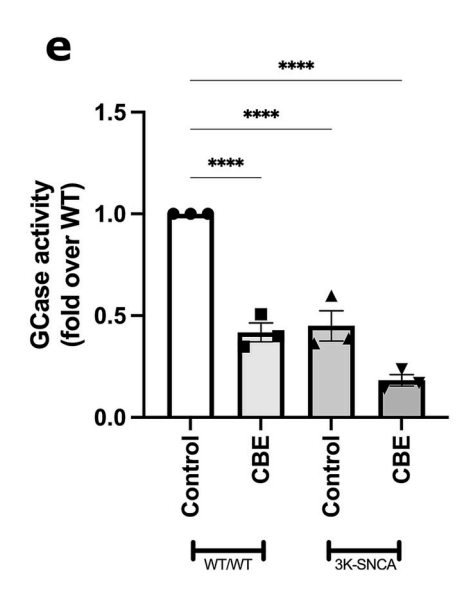


Fig. 1. Characterisation of SH-SY5Y overexpressing 3 K-SNCA mutant gene. a,b) Representative images showing a-synuclein inclusions in 3 K-SNCA cells compared to wild-type SH-SY5Y. Blue: DAPI. Green: a-synuclein inclusions. White arrows point to a-synuclein inclusions. c) Quantification of a-synuclein inclusions in 3 K-SNCA cells vs wild-type SH-SY5Y. 3 K-SNCA cells developed at least one cytoplasmatic a-synuclein inclusion, as opposed to the control group, showing less than 0.01 inclusions/cytoplasm. Data of three independent experiments (N = 3), with 8 technical replicates per condition in each experiment (n = 24). Normal distribution. Two-tailed t-test. (T value14.69, degrees of freedom 2.00) Mean  $\pm$  SEM. \*\*p = 0.0046. d) HTRF-FRET quantification of a-synuclein aggregates in parental SH-SY5Y and 3 K-SNCA overexpressing cells, showing a ratio fold change of 1.458 in 3 K-SNCA cells vs wild type. Data of three independent experiments (N = 3), with 3 technical replicates per condition in each experiment (n = 9). Non-normal distribution. Mann-Whitney test (U value 0). Mean  $\pm$  SEM. \*\*\*\*p = 0.0015. e) Quantification of total GCase activity in 3 4-SNCA and wild type SH-SY5Y, including irreversible GCase inhibitor Conduritol B epoxide (CBE). Treatment with CBE at 300 p = 30 p = 30

as increased a-synuclein accumulation results in selective reduction of GCase activity and protein levels in synucleinopathies (Gegg et al., 2012). We quantified GCase activity in cell lysates, finding an approximate 50 % reduction in *3 K-SNCA* (Fig. 1; e). Additionally, we validated our findings by treating the cells with the irreversible GCase inhibitor Conduritol B epoxide (CBE), thereby confirming the specificity of GCase-related effects. This result confirms that overexpression of mutant asynuclein and formation of inclusions compromises wild-type GCase activity, recapitulating previous results (Stojkovska et al., 2022).

3.2. PIKfyve-inhibitor reduces a-synuclein inclusions via lysosomal pathway

We tested the effects of PIKfyve-inhibitor YM201636 on a-synuclein accumulation in 3 K-SNCA cells. To identify the optimal drug dosage, we treated 3 K-SNCA cells with serial concentrations of YM201636 for 24 h, using as readout the total number of a-synuclein inclusions/cell. Our results indicate that YM201636 treatment displayed a trend towards a decrease in the number of inclusions at  $1~\mu M$  (Fig.S1), a concentration

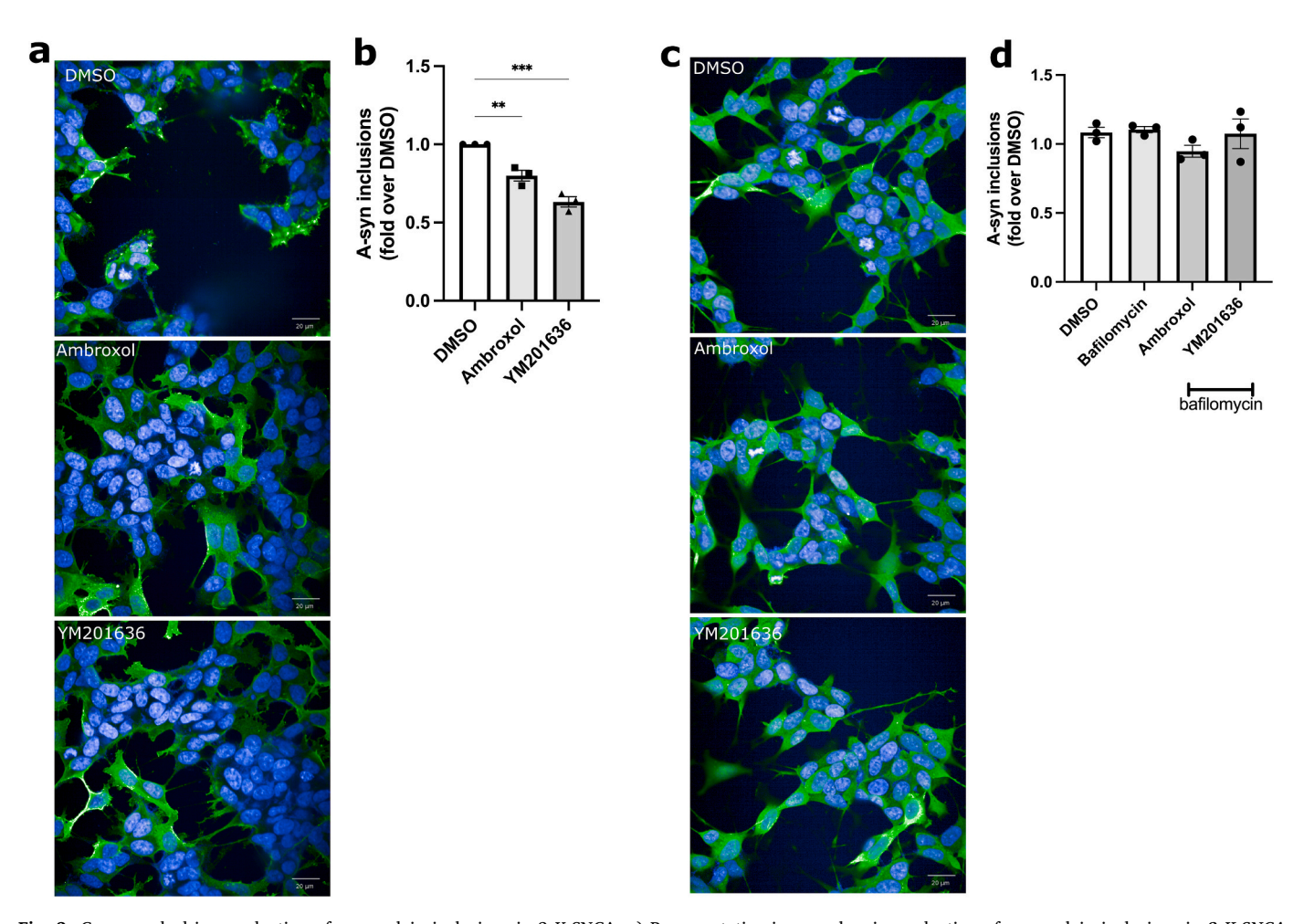


Fig. 2. Compounds-driven reduction of a-synuclein inclusions in 3 K-SNCA. a) Representative images showing reduction of a-synuclein inclusions in 3 K-SNCA treated cells compared to vehicle control. Blue: DAPI (blue). Green (488 channel): a-synuclein inclusions. b) A-synuclein inclusions quantification in 3 K-SNCA cells following treatment. Data represented as fold-change over vehicle control. Normally distribution. ANOVA one-way test (F value 45.3, total degrees of freedom 8). Mean  $\pm$  SEM. Data from 3 independent experiments (N = 3) with 3 technical replicates per condition in each experiment (n = 9). \*\*P = 0.009; \*\*\*P < 0.0001. c) Representative images showing inhibition of reduction of a-synuclein inclusions for ambroxol and YM201636 following treatment with bafilomycin-A1. Blue: DAPI. Green (488 channel): a-synuclein. d) Quantification of a-synuclein inclusions in 3 K-SNCA following co-treatment with 10 nM bafilomycin-A1 for 24 h. Normal distribution. ANOVA one-way (F value 1.31, total degrees of freedom 11). Mean  $\pm$  SEM. Data from 2 independent experiments (N = 2) with 3 technical replicates per condition in each experiment (n = 6). (For interpretation of the references to colour in this figure legend, the reader is referred to the web version of this article.)

that has previously been shown to inhibit the PIKfyve pathway (Hasegawa et al., 2022). 3 K-SNCA cells were treated with 1  $\mu$ M of YM201636 or a vehicle control for 24 h. Ambroxol, an oral mucolytic drug that acts as a pH-dependent, mixed-type inhibitor of GCase (Maegawa et al., 2009; McNeill et al., 2014), has been reported to be capable of modulating TFEB (Magalhaes et al., 2018). Consequently, as a drug control, ambroxol treatment was administered at 30  $\mu$ M, as previously reported (Magalhaes et al., 2018), resulting in approximately 20% decrease of inclusions. PIKfyve-inhibition by YM201636 also produced a significant reduction, with the number of a-synuclein inclusions being reduced by 37% (Fig. 2; a,b).

Since YM201636 has been reported to induce TFEB nuclear translocation (Choy et al., 2018), we investigated whether: (i) TFEB stimulation effects are exerted, to some extent, through the lysosomal system, and (ii) lysosomal function mediates the reduction of a-synuclein inclusions under TFEB stimulation. We treated 3 K-SNCA cells with bafilomycin-A1, which de-acidifies the lysosome by inhibiting the vacuolar-type ATPase in the lysosomal membrane, impairing lysosomal function (Fedele and Proud, 2020). No significant reduction of inclusions was achieved by YM201636 or ambroxol when coadministrated with bafilomycin-A1 (Fig. 2; c-d), confirming that lysosomal function contributes to the reduction in a-synuclein induced by YM201636.

### 3.3. PIKfyve-inhibition treatment increases TFEB nuclear translocation and subsequent lysosomal biogenesis

We next investigated whether an increase in nuclear TFEB levels was detectable following treatment with YM201636 and ambroxol. A statistically significant increase of approximately 73 % and 30 % was detected after 24 h of treatment for both ambroxol and YM201636 respectively (Fig. 3; a-e). To test whether this enhanced TFEB nuclear levels resulted in an increase in cellular lysosomal density, we quantified GCase protein using a high-content imaging approach. A significant increase in GCase levels in 3 K-SNCA treated cells was seen with ambroxol and YM201636 after 24 h. Our analysis did not reveal any significant increase in GCase activity at this stage in any group (Fig.S2; a-c).

To investigate further whether ambroxol and YM201636 treatments modulate overall lysosomal biogenesis, we quantified the presence of the Lysosomal Associated Membrane Protein 1 (LAMP1). This lysosomal external membrane protein is distributed among autophagic and endolysosomal organelles and LAMP1-positive organelles are routinely referred to as lysosomal compartments (Cheng et al., 2018). Our analysis showed that PIKfyve-inhibition significantly increased LAMP1 punctate levels after 24 h. Conversely, ambroxol did not result in an overall increase in LAMP1, with effects limited to GCase (Fig. 3; f-g). Furthermore, to assess the capability of YM201636 to enhance the autophagic degradation capacity of 3 K-SNCA cells, we performed an analysis of cargo degradation using a DQ-BSA assay. YM201363 treated cells showed a significant increase in cargo degradation compared to vehicle control (Fig. 3; h, i).

Additionally, we examined the CLEAR network. qPCR analysis for a TFEB-target gene containing the CLEAR motif in their promotor (namely HEXA, a gene that encodes a lysosomal enzyme which TFEB targets via the CLEAR pathway) (Palmieri et al., 2011). There was no statistically significant change in the regulation of HEXA expression level in 3 K-SNCA cells treated with YM201636 compared to vehicle control (Fig. S3). Additionally, no increased expression was detected in the GLA gene, which is not regulated by TFEB.

Together, these data support the proposal that YM201636-induced reduction of a-synuclein is mediated through promoting nuclear TFEB translocation, ultimately increasing the pool of lysosomes and the general degradative capacity of lysosomes. However, this is not associated with an increment of global GCase activity.

### 3.4. PIKfyve-inhibition reduces a-synuclein burden via TFEB in differentiated 3 K-SNCA overexpressing cells

Although SH-SY5Y cells constitute a valuable asset to study the molecular complexity of PD, this cell line was obtained as a neuroblastoma derivative and, as a consequence, it has cancerous features that influence its differentiation fate, viability, growth performance, metabolic properties and genomic stability. Hence, SH-SY5Y cells possess physiological characteristics which differ greatly from the normal dopaminergic neuronal properties (Xicoy et al., 2017). One of the main limitations of SH-SY5Y is its active cellular division, which results in changes in lysosomal activity and composition, opposite to what is observed in neuronal cells where a constant G0 phase of the cell cycle is present (Shipley et al., 2016).

To investigate whether our findings would be recapitulated in 3 *K-SNCA* cells without active division, we obtained derivative cells with a neuronal phenotype by using a retinoic acid and brain-derived neurotrophic factor induced differentiation protocol (Gegg et al., 2020; Uras et al., 2022). This procedure leads to a homogeneous neuronal population with expression of neuronal markers and decreased proliferation (Encinas et al., 2000). After 10 days in culture, SH-SY5Y overexpressing 3 *K-SNCA* cells exhibited a neuronal morphology and markers (Fig.S4), with the presence of cytoplasmatic a-synuclein inclusions (Fig. 4; a). In differentiated 3 *K-SNCA*-SH-SY5Y, YM201636 was able to induce a significant reduction in a-synuclein inclusions after 24 h of treatment (Fig. 4; b).

To confirm that YM201636 was acting through a TFEB-mediated pathway, we investigated nuclear TFEB levels at different time points. Our results confirm that YM201636 treatment was able to significantly increase nuclear TFEB by 48 %, and the effect was more rapid than in undifferentiated cells, established at 7 h (Fig. 5; a-c). Examination of the CLEAR network by qPCR analysis showed a significant upregulation in the expression level of *HEXA* (approximately 6-fold) in *3 K-SNCA* cells treated with YM201636 compared to vehicle control (Fig. 5; d-e). No increased expression was detected in the non-TFEB regulated *GLA* control gene. These results confirm that TFEB nuclear translocation induced by PIKfyve-inhibition resulted in activation of the CLEAR network.

We did not detect any significant increase in GCase cytoplasmatic protein levels or activity after 24 h YM201636 treatment (Fig.S5). LAMP1 punctates were significantly increased after PIKfyve-inhibition (Fig. 5; f-g). The size of the *endo*-lysosomal compartment in the differentiated cells was analysed by Lysotracker® staining and showed a significant increase in YM201636 treated cells compared to vehicle control (Fig. 5; h, i). However, cargo degradation analysis did not show increased lysosomal degradative capacity in treated cells (Fig. 5; j, k).

These results indicate that the PIKfyve-inhibitor YM201636 enhanced TFEB nuclear translocation, resulting in an increase in LAMP1 levels, upregulation of *HEXA* gene expression and increased lysosomal compartment. Nonetheless, no significant changes in GCase levels, GCase activity or overall lysosomal degradative capacity were detected.

### 3.5. PIKfyve-inhibition reduces a-synuclein burden in A53T hiPSC-derived dopaminergic neurons

We then used iPSCs-derived dopaminergic neurons (Fujifilm Cellular Dynamics Inc) with a heterozygous gene-edited p.A53T mutation (iCell A53T DOPA) and isogenic controls (iCell DOPA) to examine further the effects and mechanism of action of YM201636.

After 17 days *in vitro*, a highly significant increase in a-synuclein inclusions was detected in the p.A53T neurons compared to their isogenic control (Fig. 6; a,b). We, then, tested the effect of YM201636 on a-synuclein inclusion formation. In this case, a longer treatment scheme of 7 days at 1  $\mu$ M YM201636 was used as these cells are not dividing and so require a longer period of exposure than dividing cells. PIKfyve inhibition significantly decreased the levels of inclusions by 19 % when

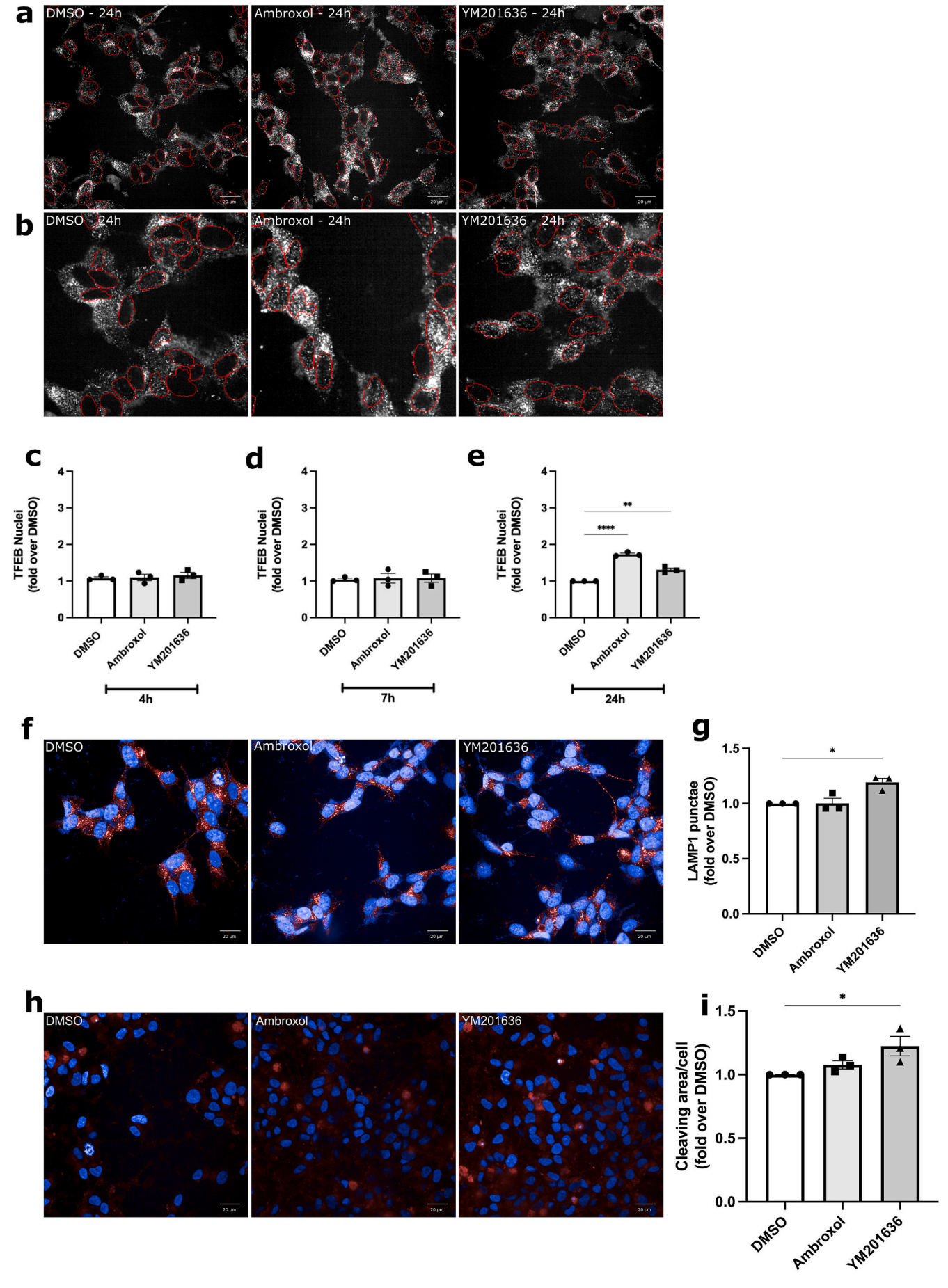


Fig. 3. Compounds-driven increase of TFEB nuclear levels and lysosomal compartment. a, b) Representative images showing increased nuclear TFEB after 24 h of compound treatment in wild-type (a) and 3 K-SNCA (b) SH-SY5Y cells. Nuclei delimited by red line. White spots: TFEB. c) TFEB nuclear signal intensity quantification after 4 h treatment in 3 K-SNCA cells. ANOVA one-way. Mean  $\pm$  SEM. Data from three independent (N = 3) experiments with 3 technical replicates per condition in each experiment (n = 9). d) TFEB nuclear signal intensity after 7 h treatment in 3 K-SNCA cells. ANOVA one-way. Mean  $\pm$  SEM. Data from three independent experiments (N = 3) with 4 technical replicates per condition in each experiment (n = 12). e) Quantification of TFEB nuclear signal intensity after 24 h treatment in 3 K-SNCA cells. Normal distribution. ANOVA one-way (F-value 121.9, degrees of freedom 8). Mean  $\pm$  SEM. Data of three independent experiments (N = 3), with 4 technical replicates per condition in each experiment (n = 12). \*\*P = 0.003; \*\*\*\*\*P < 0.0001. f) Representative images of increased LAMP1 levels after compounds exposure in 3 K-SNCA cells. Blue: DAPI. Red: LAMP1. g) LAMP1 quantification after 24 h of compound treatment in 3 K-SNCA cells, showing a 10 % increase in LAMP1 punctate levels in YM201636-treated cells compared to vehicle control. Non-normal distribution. Kruskal-Wallis (H value 6.28). Mean  $\pm$  SEM. Data of three independent experiments (N = 3), with 4 technical replicates per condition in each experiment (n = 12). \*\*P = 0.013. h) Representative images of DQ-BSA analysis in 3 K-SNCA cells. i) DQ-BSA area in treated 3 K-SNCA cells. Normal distribution. ANOVA one way (F-value 5.705, total degrees of freedom 8). Mean  $\pm$  SEM. Data of three independent experiments (N = 3), with 9 technical replicates per condition in each experiment (n = 27). \*\*P = 0.028. (For interpretation of the references to colour in this figure legend, the reader is referred to the web version of this article.)

compared to vehicle control (Fig. 6; c,d).

We also measured the lysosomal compartment by analysing the Lysotracker® staining fluorescent intensity. Our data showed a significant increase in the endo-lysosomal area (Fig. 6; e,f).

#### 4. Discussion

In the present study, we report that 3 K-SNCA SH-SY5Y cells show an approximate 50 % decrease in GCase activity compared to the wild-type, in agreement with earlier characterisations of SNCA overexpressing models. Gegg et al. (2012) showed a decrease in both GCase activity and protein levels by 70 % and 87 %, respectively, in human SH-SY5Y overexpressing high levels of exogenous a-synuclein. Moreover, hippocampal and cortical neurons and differentiated dopaminergic SH-SY5Y have been reported to display decreased GCase activity when treated with preformed a-synuclein fibrils (PFF) (Gegg et al., 2020; Henderson et al., 2020). Importantly, the neuroblastoma cells transiently transfected with 3 K-SNCA have been reported to exhibit marked ER stress (Ericsson et al., 2021), consistent with our findings of reduced GCase activity, and consequently reduced lysosome hydrolase catabolism, further confirming parallels with the PD phenotype in the 3 K-SNCA cell model. The relationship between lysosomal dysfunction, a-synuclein misfolding, aberrant clearance and ultimately its toxic aggregation has been previously reported (Klein and Mazzulli, 2018; Mazzulli et al., 2011; Mazzulli et al., 2016).

We have studied the role of the small-molecule PIKfyve inhibitor YM201636 in reducing cytoplasmatic a-synuclein inclusions in 3 K-SNCA cells and hiPSC-derived neurons. Our results demonstrate a decrease of a-synuclein inclusions in all models, independently of the cell type. Furthermore, in *3 K-SNCA* cells this is mediated with TFEB nuclear localisation linked to lysosomal biogenesis.

In *3 K-SNCA* cells, the mutations generate cytoplasmic inclusions comprising clusters of lipid droplets, endocytic vesicles, and a-synuclein

(Ericsson et al., 2021), with short tubular structures rich in a-synuclein with no evidence for fibrillar a-synuclein either in or associated with the inclusions (Dettmer et al., 2017). Lewy bodies may exist as predominantly proteinaceous, fibrillar lesions (Spillantini et al., 1998); however, there is ongoing debate regarding the disease-relevance of non-fibrillar Lewy bodies (Lashuel, 2020). Our observation that PIKfyve inhibition reduces inclusions in 3 K-SNCA cells expressing large amounts of membrane-enriched a-synuclein that do not seem to form obvious fibrillar aggregates, is therefore of interest.

In undifferentiated cells, the a-synuclein increase was partially reversed following a short-duration treatment with YM201636. The mechanism of action was reliant on lysosomal function, as no reduction of a-synuclein inclusions occurred when co-administrated with bafilomycin-A1. Additionally, PIKfyve-kinase inhibition resulted in an increased presence of TFEB in the nucleus after 24 h of treatment, indicating enhanced TFEB nuclear translocation. Ambroxol showed similar results. LAMP1 punctate intensity was elevated, indicating an increase in the number and volume of the lysosomal compartment, and further demonstrating the lysosomal-dependent mechanism of YM201636. In the case of the biogenesis of new and functional lysosomes, lysosomal activity should increase in line with lysosome quantity and volume. For this reason, we performed analysis of cargo degradation by DQ-BSA, which has the advantage of assessing the general degradative capacity of lysosome as a whole and not of a specific lysosomal enzyme activity. Our studies showed an increase in the cleavage of substrate, demonstrating an enhanced lysosomal catabolism after PIKfyve-inhibition. This observation supports the proposal that the mechanism of action of PIKfyve inhibition involves a stimulation of autophagy, making the cellular machinery capable of degrading inclusions independently of the a-synuclein conformation present in them.

Our findings demonstrate a global increase in lysosomal LAMP1 puncta and enhanced cargo degradation, which may contribute to the improvement of cellular clearance mechanisms. Nonetheless, despite

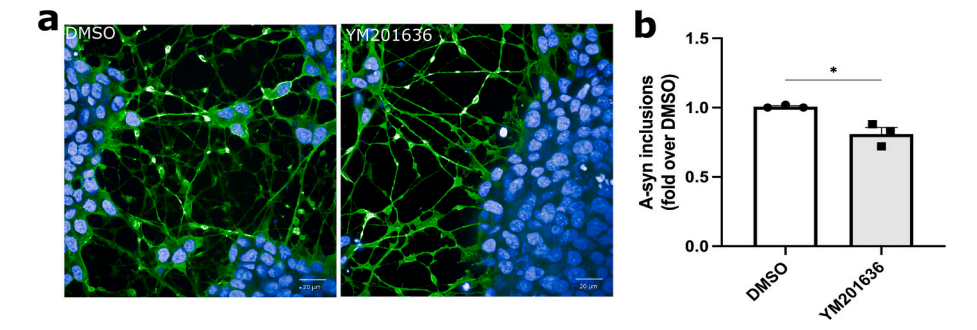
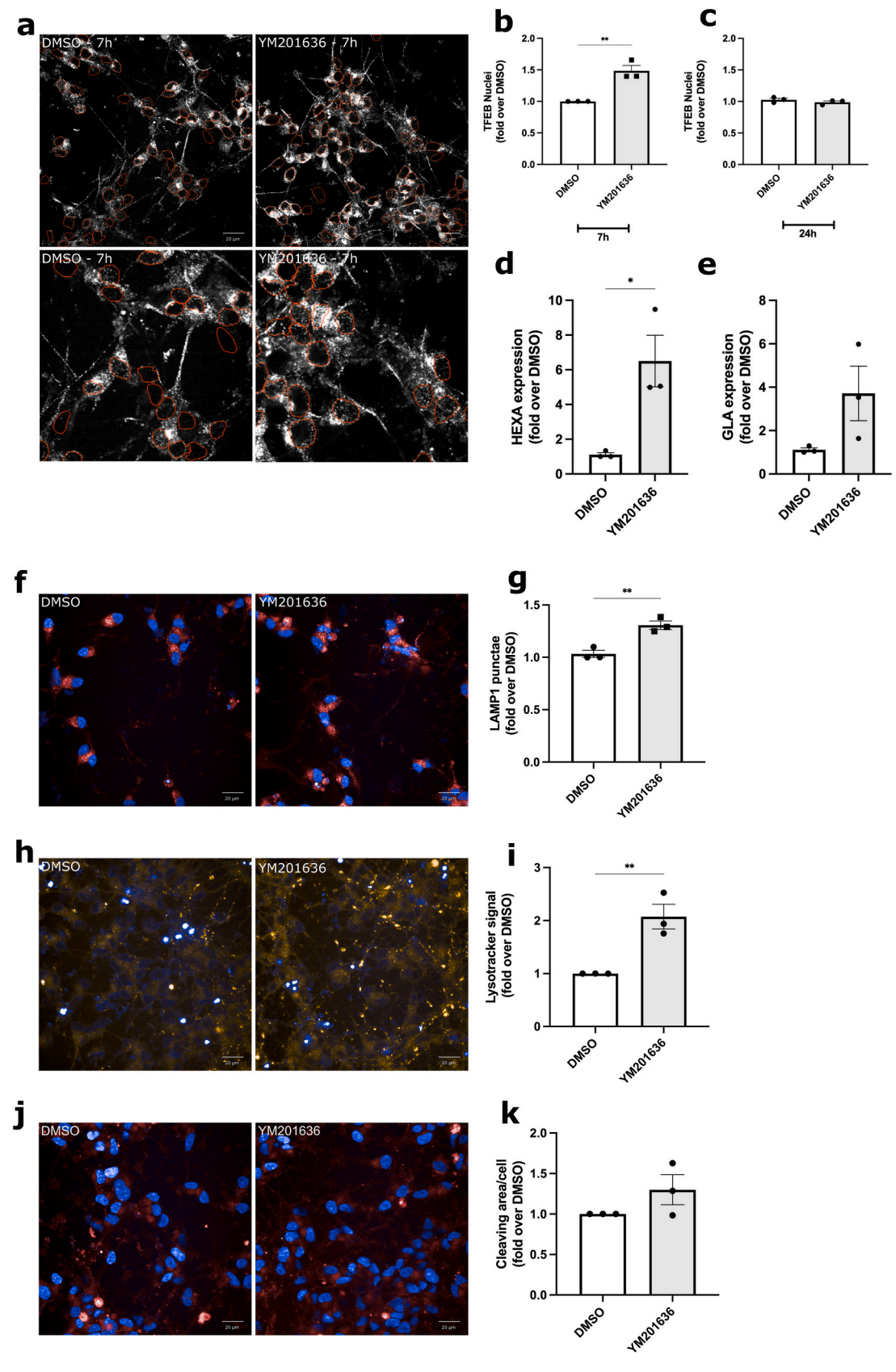


Fig. 4. Characterisation of differentiated SH-SY5Y overexpressing 3 K-SNCA. a) Representative images showing reduction of a-synuclein inclusions in differentiated 3 K-SNCA cells treated with YM2011636 compared to vehicle control. Blue: DAPI. Green: a-synuclein aggregates. b) Quantification of a-synuclein spots in 3 K-SNCA differentiated cells after YM2011636 treatment compared to vehicle control, showing a 23 % decrease in treated cells compared to vehicle control. Normal distribution. t-test two tailed (T value 4.12, degrees of freedom 4). Mean  $\pm$  SEM. Data of three independent experiments (N = 3), with 6, 6 and 5 technical replicates per condition in the three independent experiments respectively (n = 16). \*P = 0.02. (For interpretation of the references to colour in this figure legend, the reader is referred to the web version of this article.)



(caption on next page)

Fig. 5. Compounds-driven increase of nuclear TFEB nuclear, CLEAR pathway and lysosomal compartment in differentiated cells. a) Representative images showing increased TFEB into the nuclei after 7 h treatment in differentiated wild-type (top row) and 3-K SNCA (bottom row) SH-SY5Y cells. Nuclei delimited by red line. White spots: TFEB, b, c) Quantification of TFEB nuclear signal intensity in differentiated 3 K-SNCA cells after 7 h treatment (b) and after 24 h treatment (c). Normal distribution. t-test two tailed (T-value 5.66, degrees of freedom 4). Mean  $\pm$  SEM. Data of three independent experiments (N = 3), with 4 technical replicates per condition in each experiment (n = 12). \*\*\*P = 0.0048. d) RT-qPCR analysis of differentiated 3 K-SNCA cells showing expression of the TFEB-target gene HEXA (Hexosaminidase A). Non-normal distribution. Mann-Whitney test (U-value 0). Mean  $\pm$  SEM. Data of three independent experiments (N = 3), with 3 technical replicates per condition in each experiment (n = 9). \*P = 0.0224. e) Expresion of non-TFEB modulated lysosomal gene GLA (Galactosidase Alpha) in differentiated 3 K-SNCA cells. Mann-Whitney test t-test two tailed. Mean  $\pm$  SEM. Data of three independent experiments (N = 3), with 3 technical replicates per condition in each experiment (n = 9). f) Representative confocal images showing increased LAMP1 levels after YM201636 treatment in differentiated 3 K-SNCA cells. Blue: DAPI. Red: LAMP1. g) Quantification of LAMP1 punctate per cell after 24 h of YM201636 treatment in differentiated 3 K-SNCA cells when compared to vehicle control. Normal distribution. Two-tailed t-test (T-value 5.262, degrees of freedom 4). Mean  $\pm$  SEM. Data of three independent experiments (N = 3), with 4 technical replicates per condition in each experiment (n = 12). \*\*P = 0.0062. h) Images of Lysotracker® staining in differentiated 3 K-SNCA cells treated with YM201636 or vehicle control. i) Lysotracker® signal quantification in treated differentiated 3 K-SNCA cells. Normal distribution. Two-tailed t-test (T-value 4.61, degrees of freedom 4). Mean  $\pm$ SEM. Data of three independent experiments (N = 3), with 4 technical replicates per condition in each experiment (n = 12). \*\*P = 0.0099. j) Representative images of DQ-BSA analysis in differentiated 3 K-SNCA cells. k) DQ-BSA area quantification in YM201636-treated differentiated 3 K-SNCA cells vs vehicle control. Data is shown as mean  $\pm$  SEM. Data of three independent experiments (N = 3), with 4 technical replicates per condition in each experiment. Mann-Whitney test (n = 12). (For interpretation of the references to colour in this figure legend, the reader is referred to the web version of this article.)

the fact that YM201636 stimulated TFEB nuclear translocation with an eventual reduction of a-synuclein, this stimulation could potentially not fully compensate for the GCase activity reduction induced by a-synuclein accumulation. Previous studies have reported that, in mouse cortical neurons, while the majority of lysosomal hydrolases colocalise with LAMP1, a portion of LAMP1-labeled organelles do not contain detectable lysosomal hydrolases, including GCase, representing early endo-lysosomal structures which have still not reached a full degradative status (Cheng et al., 2018). Additionally, previous research showed that SNCA overexpression causes a-synuclein accumulation at the ER where it could impair proteostasis capacity (Stojkovska et al., 2022), sequestering chaperones away from their normal function. Moreover, a-synuclein can directly impair protein trafficking machinery to the Golgi (Stojkovska et al., 2022), causing a downstream lysosomal depletion. Although this effect in synucleinopathies is not hydrolase specific, some hydrolases are more susceptible than others. GCase is particularly vulnerable to aggregation because of prolonged folding cycles that result in abnormal exposure of hydrophobic domains (Stojkovska et al., 2022). Consequently, we hypothesise that this lack of effect in GCase activity could be attributed to enhanced aggregation of a-synuclein at the ER, causing ER fragmentation, compromising folding capacity and aggregation of lysosomal hydrolases in the ER (Stojkovska et al., 2022) and, hence, causing accumulation of immature forms of GCase in the ER and reduction of protein functionality.

Even though SH-SY5Y cells constitute a valuable asset to study the molecular complexity of PD, this cell line is a neuroblastoma derivative and, consequently, it possess physiological characteristics which differ greatly from the constitutive dopaminergic neuronal properties in differentiation fate, viability, growth performance, metabolic properties and genomic stability (Xicoy et al., 2017). One of the main limitations of SH-SY5Y is its active cellular division, which results in changes in lysosomal activity and composition, opposite to what is observed in neuronal cells (Shipley et al., 2016). To overcome this, we differentiated 3 K-SNCA cells into a neuron-like phenotype (Uras et al., 2022). This differentiation did not affect the presence of a-synuclein inclusions, corroborating the existence of a-synuclein-induced lysosomal dysfunction. Short-treatment PIKfyve-inhibition resulted in a significant reduction of a-synuclein inclusions and increase in TFEB nuclear incorporation. We also detected a significant upregulation of the TFEBtarget gene tested, with no significant increase in non-TFEB mediated gene expression, confirming that TFEB nuclear translocation induced by PIKfyve-inhibition led to an activation of the CLEAR network. Consistent with these results, LAMP1 punctuate, and the size of the endo-lysosomal compartment were elevated, confirming the lysosomal-conditioned mechanism of action of PIKfyve inhibition. Nonetheless, GCase protein levels and activity did not change, which could potentially be explained by enhanced aggregation of a-synuclein at the ER (Stojkovska et al., 2022).

Finally, we confirmed PIKfyve inhibition-mediated reduction of asynuclein inclusions in patient-derived iPSC-differentiated dopaminergic neurons carrying the PD-associated p.A53T point mutation in SNCA. In contrast to the *3 K-SNCA* mutation, the nature of the p.A53T asynuclein promotes a-synuclein oligomerisation and fibrillation *in vitro* (Lemkau et al., 2013) and displays enhanced PD-like pathology in animal and cellular models (Giasson et al., 2002), mainly due to changes of the paring geometry of protofilaments of the fibril, and thus changing morphology of the mature fibril (Sun et al., 2020).

We applied a 7-day drug exposure in dopaminergic neurons due to slow protein turnover and aggregation dynamics. Pathological a-synuclein inclusions form gradually, and sustained treatment is needed for effective clearance (Yang et al., 2022). Additionally, it has been reported that longer treatment schemes with PIKfyve modulators are capable of enhancing lysosomal biogenesis and production of lysosomal hydrolases in fibroblasts (Hou et al., 2024). PIKfyve inhibiton enhances a-synuclein degradation via autophagy and lysosomal pathways, which requires time for full activation. Short-term exposure may not reflect true efficacy, as it may miss compensatory effects.

We report a significant reduction in a-synuclein inclusions in A53T dopaminergic neurons, confirming that PIKfyve modulation is capable of reducing a-synuclein aggregates in a PD-associated neuronal cell model, and confirming this pathway as being important for a-synuclein clearance.

We observed a 19 % increase in lysosomal signal intensity, as measured by LysoTracker® staining, in A53T dopaminergic neurons following treatment with YM201636. This finding suggests that modulating PIKfyve enhances lysosomal biogenesis in this PD neuronal model. This enhancement reinforces the significance of lysosomal pathways in the clearance of a-synuclein. The increase in the size of the endolysosomal compartment after treatment with YM201636 aligns with previous studies indicating that PIKfyve modulation can lead to increased lysosomal biogenesis (Hou et al., 2024). The observed increase in lysosomal signal intensity may represent an early adaptive response aimed at restoring lysosomal function in neurons carrying the p.A53T asynuclein, emphasising the significance of lysosomal pathways in the clearance of a-synuclein. Future studies employing longer treatment durations and additional markers of lysosomal biogenesis will be required to further clarify the effects of PIKfyve inhibition on lysosomal function in mature dopaminergic neuronal models.

The experiments conducted in A53T cells provide preliminary evidence supporting the efficacy of PIKfyve inhibition in reducing a-synuclein levels. However, one limitation of the p.A53T cell model is the study of post-treatment TFEB nuclear levels, since quantification of TFEB could not be investigated due to the timeline of the experiment. TFEB is degraded through the proteasome pathway in both neuronal-like and non-neuronal cells (Li et al., 2019), with a half-life of approximately 13.5 h in neuronal-like cells. For this reason, TFEB levels were

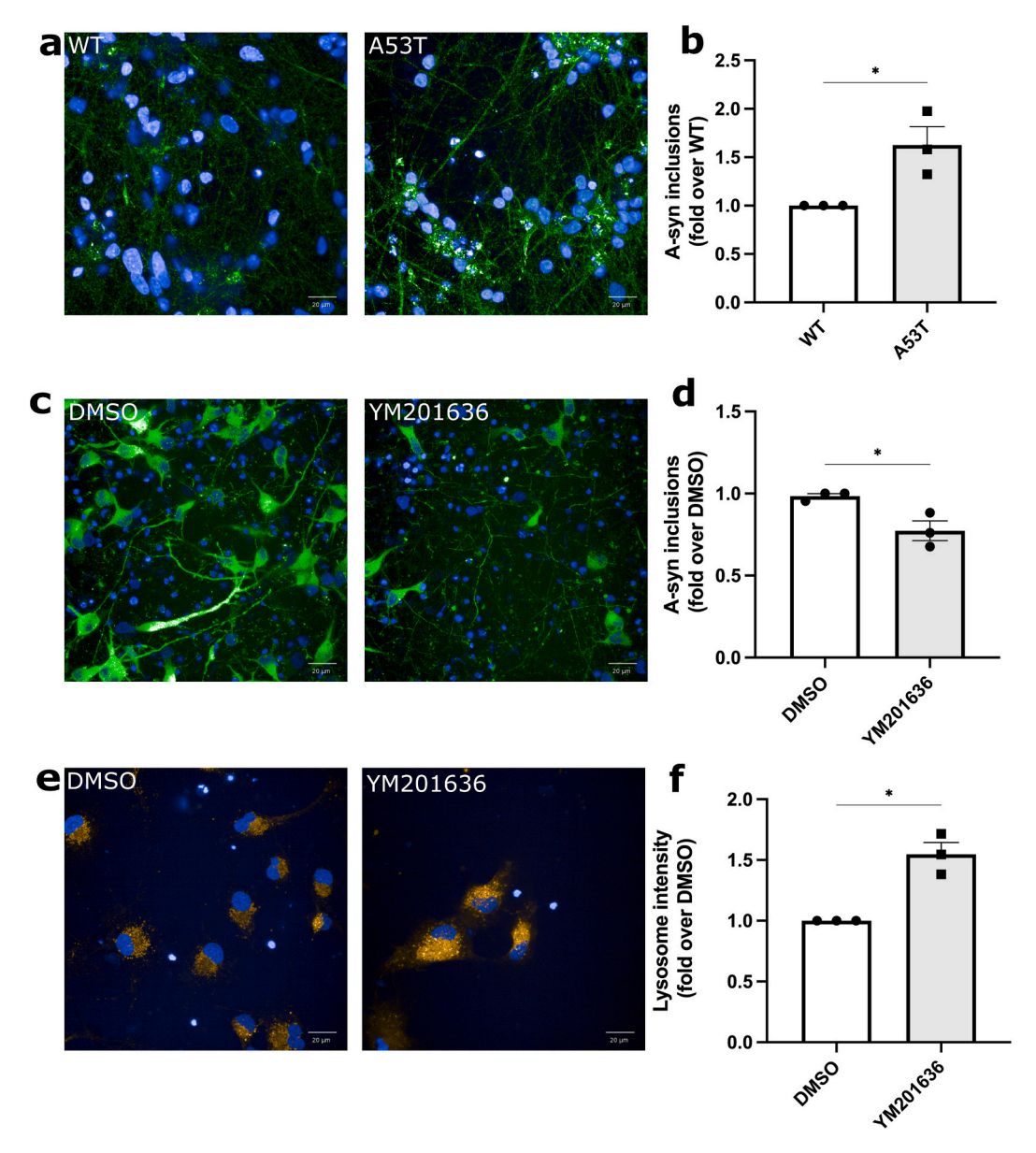


Fig. 6. PIKfyve inhibition reduction of a-synuclein inclusions in iCell A53T DOPA cells. a) Representative images of a-synuclein inclusions in iPSCs-derived dopaminergic neurons with a heterozygous gene-edited p.A53T mutation (A53T) and isogenic controls (WT). b) Quantification of a-synuclein inclusions in iPSCs-derived dopaminergic neurons with heterozygous gene-edited p.A53T mutation (A53T) and isogenic controls (WT). Non-normal distribution. Mann-Whitney test (U-value 0). Mean  $\pm$  SEM. Data of three independent experiments (N = 3), with 4 technical replicates per condition in each experiment (n = 12). \* $^{*}P = 0.023$ . c) Representative images of a-synuclein inclusions A53T dopaminergic neurons treated with YM201636 and vehicle control (DMSO). d) Quantification of a-synuclein inclusions A53T dopa-neurons treated with YM201636 vs vehicle control. Normal distribution. Two tailed t-test (T-value 3.421, degrees of freedom 4). Mean  $\pm$  SEM. Data of three independent experiments (N = 3), with 3 technical replicates per condition in each experiment (n = 12). \* $^{*}P = 0.026$ . e) Representative images of Lysotracker® staining in A53T dopa-neurons treated with DMSO or YM20163. f) Quantification of Lysotracker® intensity signal in A53T dopa-neurons treated with DMSO or YM20163. Normal distribution. Two-tailed t-test (T-value 5.683, degrees of freedom 4). Mean  $\pm$  SEM. Data of three independent experiments (N = 3), with 3 technical replicates per condition in each experiment (n = 9). \* $^{*}P = 0.29$ .

undetectable after seven days. Further research to explore the effects of PIKfyve inhibition by YM201636 in dopaminergic neurons in warranted.

TFEB is highly expressed in the central nervous system (Cortes and La Spada, 2019). Defective neuronal clearance of autophagic substrates and aggregate-prone proteins has been associated with impaired TFEB localisation and function in PD (Cortes and La Spada, 2019; Decressac et al., 2013), including GBA1-associated PD (Mubariz et al., 2023). For this reason, our work attempted to prevent pathological a-synuclein inclusion formation by treating *3 K-SNCA* cells with the PIKfyve-inhibitor YM201636 to enhance lysosomal biogenesis via TFEB. Our results consistently show increased nuclear TFEB localisation after

treatment with YM201636, consequently stimulating the transcription of the genes included in the CLEAR pathway and eventually reducing the number of a-synuclein inclusions. Previous studies have suggested that *in vivo* overexpression of a-synuclein induced dynamic changes in TFEB, initially promoting its nuclear translocation, but sequestering TFEB into the cytoplasm when cell death occurs (Decressac et al., 2013). This modification in TFEB subcellular localisation correlated with a progressive decline in lysosome markers. Interestingly, TFEB colocalised with a-synuclein and was observed in Lewy body-containing nigral neurons in human brains of people with PD (Decressac et al., 2013). Transgenic technology to induce TFEB overexpression and pharmacological activation of TFEB was able to restore lysosomal biosynthesis and

reduce accumulation of aggregated a-synuclein by promoting its autophagic clearance (Kilpatrick et al., 2015). While this could, at first, be a protective response to the formation of a-synuclein inclusions, the increase in lysosomal metabolism is not potentially capable of reducing a-synuclein sufficiently. Eventually, TFEB translocation is inhibited concomitantly with cell death. Consequently, increasing lysosomal biogenesis via TFEB upregulation represents a plausible disease-modifying strategy. Here, we present evidence that YM201636 is capable of significantly promoting TFEB nuclear localisation *in vitro*, with an ultimate reduction of a-synuclein inclusions, confirming the potential therapeutic value of PIKfyve modulation specifically in synucleopathies.

It is important to note that, although genetic ablation of PIKfyve can impair neurodevelopment (Ikonomov et al., 2011), and mutations in the Vac14 and/or Fig4 of the PIKfyve-complex are associated with neurodegenerative diseases such as Charcot-Marie-Tooth syndrome (Chow et al., 2007) and amyotrophic lateral sclerosis (ALS) (Osmanovic et al., 2017), the only human disease recognised to be associated with mutations in the PIKfyve-kinase gene itself is Fleck corneal dystrophy (Gee et al., 2015). This is a rare autosomal dominant ocular dystrophy not associated with neurodegeneration, confirming that partial reduction of PIKfyve activity is viable. PIKfyve inhibition by the small molecule apilimod has recently been reported following a phase 2 trial in c9orf-associated ALS and appeared to be well-tolerated (Babu et al., 2024).

It has been suggested that PIKfyve could impact TFEB independently of mTORC1 via its interaction the serine/threonine kinase Akt (protein kinase B), which modulates TFEB by phosphorylating it at Ser-467 and represses TFEB nuclear translocation (Palmieri et al., 2017). YM201636 has been proposed to inhibit Akt phosphorylation in adipocytes (Ikonomov et al., 2009), and PIKfyve-inhibition cytotoxicity in fibroblasts is evident only when the PIKfyve-inhibitor is combined with Akt signalling pathway suppression (Ikonomov et al., 2018). Potential modulation of TFEB by YM201636 via alterative mechanisms has not been entirely established and requires further research.

To conclude, this work demonstrates that activation of TFEB decreases the accumulation of aggregated a-synuclein by enhancing autophagy. This study also provides proof-of-principle evidence that the chemical modulation of the PIKfyve-TFEB axis by YM201636 is a viable potential therapeutic strategy to enhance a-synuclein aggregate degradation. PIKfyve signalling could represent a target to regulate TFEB-mediated lysosomal biogenesis.

#### Glossary

AD Alzheimer's disease

ALP Autophagy lysosomal pathway

ALS Amyotrophic Lateral Sclerosis A-synuclein Alpha-synuclein

CLEAR Coordinated Lysosomal Expression and Regulation gene

network

ER Endoplasmatic reticulum

GCase Glucocerebrosidase

hiPSC Human-induced pluripotent stem cells mTORc-1 Mechanistic target of rapamycin complex 1

PD Parkinson's disease

PIKfyve lipid kinase named after its function and domain structurephosphoinositide kinase for five position containing a FYVEfinger PIKfyve phosphorylates phosphatidylinositol-3-

phosphate (PI(3)P), producing PI(3,5)P2

PP2A Protein Phosphatase-2A

pS129 hyperphosphorylated a-synuclein at serine129

TFEB Transcription Factor EB, a member of the MiT/TFE family, is a helix-loop-helix leucine-zipper transcription factor capable of recognising sequences of the Coordinated Lysosomal Expression and Regulation gene network

CRediT authorship contribution statement

Sara Lucas-Del-Pozo: Writing - review & editing, Writing - original draft, Validation, Methodology, Investigation, Formal analysis, Conceptualization. Giuseppe Uras: Writing – review & editing, Writing - original draft, Validation, Methodology, Investigation, Formal analysis, Conceptualization. Federico Fierli: Writing - review & editing, Validation, Investigation. Veronica Lentini: Writing – review & editing, Validation, Investigation. Sofia Koletsi: Writing - review & editing, Validation, Project administration, Investigation. Carlos Lazaro-Hernandez: Writing - review & editing, Validation, Investigation. Kai-Yin Chau: Writing - original draft, Validation, Resources, Investigation. Derralynn A. Hughes: Writing – review & editing, Validation, Supervision, Methodology, Conceptualization. Anthony H.V. Schapira: Writing - review & editing, Writing - original draft, Validation, Super-Methodology, vision. Resources, Funding acquisition, Conceptualization.

#### **Declaration of competing interest**

The authors declare that they have no known competing financial interests or any commercial or financial relationships that could be construed as a potential conflict of interest in relation to this manuscript.

#### Acknowledgments

This research was funded by Aligning Science Across Parkinson's [Grant number: ASAP000420] through the Michael J. Fox Foundation for Parkinson's Research. For the purpose of open access, the author has applied a CC BY 4.0 public copyright license to all Author Accepted Manuscripts arising from this submission.

#### Appendix A. Supplementary data

Supplementary data to this article can be found online at https://doi.org/10.1016/j.nbd.2025.107053.

#### Data availability

The datasets in this study are publicly available in the zenodo.org repository (doi: https://doi.org/10.5281/zenodo.10047894).

#### References

Alcalay, R.N., Wolf, P., Levy, O.A., Kang, U.J., Waters, C., Fahn, S., Ford, B., Kuo, S.H., Vanegas, N., Shah, H., Liong, C., Narayan, S., Pauciulo, M.W., Nichols, W.C., Gan-Or, Z., Rouleau, G.A., Chung, W.K., Oliva, P., Keutzer, J., Zhang, X.K., 2018. Alpha galactosidase a activity in Parkinson's disease. Neurobiol. Dis. 112, 85–90. https://doi.org/10.1016/j.nbd.2018.01.012.

Babu, S., Nicholson, K.A., Rothstein, J.D., Swenson, A., Sampognaro, P.J., Pant, P., Macklin, E.A., Spruill, S., Paganoni, S., Gendron, T.F., Prudencio, M., Petrucelli, L., Nix, D., Landrette, S., Nkrumah, E., Fandrick, K., Edwards, J., Young, P.R., 2024. Apilimod dimesylate in C9orf72 amyotrophic lateral sclerosis: a randomized phase 2a clinical trial. Brain. https://doi.org/10.1093/brain/awae109.

Bissig, C., Croise, P., Heiligenstein, X., Hurbain, I., Lenk, G.M., Kaufman, E., Sannerud, R., Annaert, W., Meisler, M.H., Weisman, L.S., Raposo, G., van Niel, G., 2019. The PlKfyve complex regulates the early melanosome homeostasis required for physiological amyloid formation. J. Cell Sci. 132 (5). https://doi.org/10.1242/ ics.229500.

Cheng, X.T., Xie, Y.X., Zhou, B., Huang, N., Farfel-Becker, T., Sheng, Z.H., 2018. Characterization of LAMP1-labeled nondegradative lysosomal and endocytic compartments in neurons. J. Cell Biol. 217 (9), 3127–3139. https://doi.org/ 10.1083/jcb.201711083.

Chow, C.Y., Zhang, Y., Dowling, J.J., Jin, N., Adamska, M., Shiga, K., Szigeti, K., Shy, M. E., Li, J., Zhang, X., Lupski, J.R., Weisman, L.S., Meisler, M.H., 2007. Mutation of FIG 4 causes neurodegeneration in the pale tremor mouse and patients with CMT4J. Nature 448 (7149), 68–72. https://doi.org/10.1038/nature05876.

Choy, C.H., Saffi, G., Gray, M.A., Wallace, C., Dayam, R.M., Ou, Z.A., Lenk, G., Puertollano, R., Watkins, S.C., Botelho, R.J., 2018. Lysosome enlargement during inhibition of the lipid kinase PIKfyve proceeds through lysosome coalescence. J. Cell Sci. 131 (10). https://doi.org/10.1242/jcs.213587.

- Cortes, C.J., La Spada, A.R., 2019. TFEB dysregulation as a driver of autophagy dysfunction in neurodegenerative disease: molecular mechanisms, cellular processes, and emerging therapeutic opportunities. Neurobiol. Dis. 122, 83–93. https://doi. org/10.1016/j.nbd.2018.05.012.
- Cuddy, L.K., Wani, W.Y., Morella, M.L., Pitcairn, C., Tsutsumi, K., Fredriksen, K., Justman, C.J., Grammatopoulos, T.N., Belur, N.R., Zunke, F., Subramanian, A., Affaneh, A., Lansbury Jr., P.T., Mazzulli, J.R., 2019. Stress-induced cellular clearance is mediated by the SNARE protein ykt6 and disrupted by alpha-Synuclein. Neuron 104 (5), 869–884 e811. https://doi.org/10.1016/j.neuron.2019.09.001.
- Cullen, V., Sardi, S.P., Ng, J., Xu, Y.H., Sun, Y., Tomlinson, J.J., Kolodziej, P., Kahn, I., Saftig, P., Woulfe, J., Rochet, J.C., Glicksman, M.A., Cheng, S.H., Grabowski, G.A., Shihabuddin, L.S., Schlossmacher, M.G., 2011. Acid beta-glucosidase mutants linked to Gaucher disease, Parkinson disease, and Lewy body dementia alter alphasynuclein processing. Ann. Neurol. 69 (6), 940–953. https://doi.org/10.1002/ana.22400.
- Decressac, M., Mattsson, B., Weikop, P., Lundblad, M., Jakobsson, J., Bjorklund, A., 2013. TFEB-mediated autophagy rescues midbrain dopamine neurons from alphasynuclein toxicity. Proc. Natl. Acad. Sci. U. S. A. 110 (19), E1817–E1826. https:// doi.org/10.1073/pnas.1305623110.
- Dettmer, U., Newman, A.J., Soldner, F., Luth, E.S., Kim, N.C., von Saucken, V.E., Sanderson, J.B., Jaenisch, R., Bartels, T., Selkoe, D., 2015a. Parkinson-causing alphasynuclein missense mutations shift native tetramers to monomers as a mechanism for disease initiation. Nat. Commun. 6, 7314. https://doi.org/10.1038/ncomms8314.
- Dettmer, U., Newman, A.J., von Saucken, V.E., Bartels, T., Selkoe, D., 2015b. KTKEGV repeat motifs are key mediators of normal alpha-synuclein tetramerization: their mutation causes excess monomers and neurotoxicity. Proc. Natl. Acad. Sci. U. S. A. 112 (31), 9596–9601. https://doi.org/10.1073/pnas.1505953112.
- Dettmer, U., Ramalingam, N., von Saucken, V.E., Kim, T.E., Newman, A.J., Terry-Kantor, E., Nuber, S., Ericsson, M., Fanning, S., Bartels, T., Lindquist, S., Levy, O.A., Selkoe, D., 2017. Loss of native alpha-synuclein multimerization by strategically mutating its amphipathic helix causes abnormal vesicle interactions in neuronal cells. Hum. Mol. Genet. 26 (18), 3466–3481. https://doi.org/10.1093/hmg/ddx227.
- Ebrahimi-Fakhari, D., Cantuti-Castelvetri, I., Fan, Z., Rockenstein, E., Masliah, E., Hyman, B.T., McLean, P.J., Unni, V.K., 2011. Distinct roles in vivo for the ubiquitinproteasome system and the autophagy-lysosomal pathway in the degradation of alpha-synuclein. J. Neurosci. 31 (41), 14508–14520. https://doi.org/10.1523/ JNEUROSCI.1560-11.2011.
- Encinas, M., Iglesias, M., Liu, Y., Wang, H., Muhaisen, A., Cena, V., Gallego, C., Comella, J.X., 2000. Sequential treatment of SH-SY5Y cells with retinoic acid and brain-derived neurotrophic factor gives rise to fully differentiated, neurotrophic factor-dependent, human neuron-like cells. J. Neurochem. 75 (3), 991–1003. https://doi.org/10.1046/j.1471-4159.2000.0750991.x.
- Ericsson, M., von Saucken, V., Newman, A.J., Doehr, L., Hoesch, C., Kim, T.E., Dettmer, U., 2021. Crowded organelles, lipid accumulation, and abnormal membrane tubulation in cellular models of enhanced alpha-synuclein membrane interaction. Brain Res. 1758, 147349. https://doi.org/10.1016/j.brainres.2021.147349.
- Fedele, A.O., Proud, C.G., 2020. Chloroquine and bafilomycin a mimic lysosomal storage disorders and impair mTORC1 signalling. Biosci. Rep. 40 (4). https://doi.org/ 10.1042/bsr20200905.
- Fujiwara, H., Hasegawa, M., Dohmae, N., Kawashima, A., Masliah, E., Goldberg, M.S., Shen, J., Takio, K., Iwatsubo, T., 2002. Alpha-Synuclein is phosphorylated in synucleinopathy lesions. Nat. Cell Biol. 4 (2), 160–164. https://doi.org/10.1038/ ncb748.
- Gan-Or, Z., Amshalom, I., Kilarski, L.L., Bar-Shira, A., Gana-Weisz, M., Mirelman, A., Marder, K., Bressman, S., Giladi, N., Orr-Urtreger, A., 2015. Differential effects of severe vs mild GBA mutations on Parkinson disease. Neurology 84 (9), 880–887. https://doi.org/10.1212/WNL.0000000000001315.
- Gee, J.A., Frausto, R.F., Chung, D.W., Tangmonkongvoragul, C., Le, D.J., Wang, C., Han, J., Aldave, A.J., 2015. Identification of novel PIKFYVE gene mutations associated with fleck corneal dystrophy. Mol. Vis. 21, 1093–1100. https://www.ncbi.nlm.nih.gov/pubmed/26396486.
- Gegg, M.E., Burke, D., Heales, S.J., Cooper, J.M., Hardy, J., Wood, N.W., Schapira, A.H., 2012. Glucocerebrosidase deficiency in substantia nigra of Parkinson disease brains. Ann. Neurol. 72 (3) 455–463. https://doi.org/10.1002/ana.23614
- Ann. Neurol. 72 (3), 455–463. https://doi.org/10.1002/ana.23614.
  Gegg, M.E., Verona, G., Schapira, A.H.V., 2020. Glucocerebrosidase deficiency promotes release of α-synuclein fibrils from cultured neurons. Hum. Mol. Genet. 29 (10), 1716–1728. https://doi.org/10.1093/hmg/ddaa085.
- Giasson, B.I., Duda, J.E., Quinn, S.M., Zhang, B., Trojanowski, J.Q., Lee, V.M., 2002. Neuronal alpha-synucleinopathy with severe movement disorder in mice expressing A53T human alpha-synuclein. Neuron 34 (4), 521–533. https://doi.org/10.1016/ s0896-6273(02)00682-7
- Hasegawa, J., Tokuda, E., Yao, Y., Sasaki, T., Inoki, K., Weisman, L.S., 2022. PP2A-dependent TFEB activation is blocked by PIKfyve-induced mTORC1 activity. Mol. Biol. Cell 33 (3), ar26. https://doi.org/10.1091/mbc.E21-06-0309.
- Hayakawa, M., Kaizawa, H., Moritomo, H., Koizumi, T., Ohishi, T., Okada, M., Ohta, M., Tsukamoto, S., Parker, P., Workman, P., Waterfield, M., 2006. Synthesis and biological evaluation of 4-morpholino-2-phenylquinazolines and related derivatives as novel P13 kinase p110alpha inhibitors. Bioorg. Med. Chem. 14 (20), 6847–6858. https://doi.org/10.1016/j.bmc.2006.06.046.
- Henderson, M.X., Sedor, S., McGeary, I., Cornblath, E.J., Peng, C., Riddle, D.M., Li, H.L., Zhang, B., Brown, H.J., Olufemi, M.F., Bassett, D.S., Trojanowski, J.Q., Lee, V.M.Y., 2020. Glucocerebrosidase activity modulates neuronal susceptibility to pathological alpha-Synuclein insult. Neuron 105 (5), 822–836 e827. https://doi.org/10.1016/j. neuron.2019.12.004.

- Hou, W.C., Massey, L.A., Rhoades, D., Wu, Y., Ren, W., Frank, C., Overkleeft, H.S., Kelly, J.W., 2024. A PIKfyve modulator combined with an integrated stress response inhibitor to treat lysosomal storage diseases. Proc. Natl. Acad. Sci. U. S. A. 121 (34), e2320257121. https://doi.org/10.1073/pnas.2320257121.
- Ikonomov, O.C., Sbrissa, D., Shisheva, A., 2009. YM201636, an inhibitor of retroviral budding and PIKfyve-catalyzed PtdIns(3,5)P2 synthesis, halts glucose entry by insulin in adipocytes. Biochem. Biophys. Res. Commun. 382 (3), 566–570. https:// doi.org/10.1016/j.bbrc.2009.03.063.
- Ikonomov, O.C., Sbrissa, D., Delvecchio, K., Xie, Y., Jin, J.P., Rappolee, D., Shisheva, A., 2011. The phosphoinositide kinase PIKfyve is vital in early embryonic development: preimplantation lethality of PIKfyve—/— embryos but normality of PIKfyve+/—mice. J. Biol. Chem. 286 (15), 13404–13413. https://doi.org/10.1074/jbc. M111 222364
- Ikonomov, O.C., Altankov, G., Sbrissa, D., Shisheva, A., 2018. PIKfyve inhibitor cytotoxicity requires AKT suppression and excessive cytoplasmic vacuolation. Toxicol. Appl. Pharmacol. 356, 151–158. https://doi.org/10.1016/j. taap. 2018.08.001
- Ikonomov, O.C., Sbrissa, D., Shisheva, A., 2019. Small molecule PIKfyve inhibitors as cancer therapeutics: translational promises and limitations. Toxicol. Appl. Pharmacol. 383, 114771. https://doi.org/10.1016/j.taap.2019.114771.
- Imberdis, T., Negri, J., Ramalingam, N., Terry-Kantor, E., Ho, G.P.H., Fanning, S., Stirtz, G., Kim, T.-E., Levy, O.A., Young-Pearse, T.L., Selkoe, D., Dettmer, U., 2019. Cell models of lipid-rich α-synuclein aggregation validate known modifiers of α-synuclein biology and identify stearoyl-CoA desaturase. Proc. Natl. Acad. Sci. 116 (41), 20760–20769. https://doi.org/10.1073/pnas.1903216116.
- Kilpatrick, K., Zeng, Y., Hancock, T., Segatori, L., 2015. Genetic and chemical activation of TFEB mediates clearance of aggregated alpha-synuclein. PloS One 10 (3), e0120819. https://doi.org/10.1371/journal.pone.0120819.
- Klein, A.D., Mazzulli, J.R., 2018. Is Parkinson's disease a lysosomal disorder? Brain 141 (8), 2255–2262. https://doi.org/10.1093/brain/awy147.
- Lashuel, H.A., 2020. Do Lewy bodies contain alpha-synuclein fibrils? And does it matter? A brief history and critical analysis of recent reports. Neurobiol. Dis. 141, 104876. https://doi.org/10.1016/j.nbd.2020.104876.
- Lees, A., 2010. The bare essentials: Parkinson's disease. Pract. Neurol. 10 (4), 240–246. https://doi.org/10.1136/jnnp.2010.217836.
- Lemkau, L.R., Comellas, G., Lee, S.W., Rikardsen, L.K., Woods, W.S., George, J.M., Rienstra, C.M., 2013. Site-specific perturbations of alpha-synuclein fibril structure by the Parkinson's disease associated mutations A53T and E46K. PloS One 8 (3), e49750. https://doi.org/10.1371/journal.pone.0049750.
- Li, C., Wang, X., Li, X., Qiu, K., Jiao, F., Liu, Y., Kong, Q., Liu, Y., Wu, Y., 2019. Proteasome inhibition activates autophagy-lysosome pathway associated with TFEB Dephosphorylation and nuclear translocation. Front. Cell Dev. Biol. 7, 170. https://doi.org/10.3389/fcell.2019.00170.
- Maegawa, G.H., Tropak, M.B., Buttner, J.D., Rigat, B.A., Fuller, M., Pandit, D., Tang, L., Kornhaber, G.J., Hamuro, Y., Clarke, J.T., Mahuran, D.J., 2009. Identification and characterization of ambroxol as an enzyme enhancement agent for Gaucher disease. J. Biol. Chem. 284 (35), 23502–23516. https://doi.org/10.1074/jbc.M109.012393.
- Magalhaes, J., Gegg, M.E., Migdalska-Richards, A., Doherty, M.K., Whitfield, P.D., Schapira, A.H., 2016. Autophagic lysosome reformation dysfunction in glucocerebrosidase deficient cells: relevance to Parkinson disease. Hum. Mol. Genet. 25 (16), 3432–3445. https://doi.org/10.1093/hmg/ddw185.
- Magalhaes, J., Gegg, M.E., Migdalska-Richards, A., Schapira, A.H., 2018. Effects of ambroxol on the autophagy-lysosome pathway and mitochondria in primary cortical neurons. Sci. Rep. 8 (1), 1385. https://doi.org/10.1038/s41598-018-19479-8.
- Marwaha, R., Sharma, M., 2017. DQ-red BSA trafficking assay in cultured cells to assess cargo delivery to lysosomes. Bio-Protoc. 7 (19). https://doi.org/10.21769/ BioProtoc.2571.
- Mazzulli, J.R., Xu, Y.H., Sun, Y., Knight, A.L., McLean, P.J., Caldwell, G.A., Sidransky, E., Grabowski, G.A., Krainc, D., 2011. Gaucher disease glucocerebrosidase and α-synuclein form a bidirectional pathogenic loop in synucleinopathies. Cell 146 (1), 37–52. https://doi.org/10.1016/j.cell.2011.06.001.
- Mazzulli, J.R., Zunke, F., Isacson, O., Studer, L., Krainc, D., 2016. Alpha-Synuclein-induced lysosomal dysfunction occurs through disruptions in protein trafficking in human midbrain synucleinopathy models. Proc. Natl. Acad. Sci. U. S. A. 113 (7), 1931–1936. https://doi.org/10.1073/pnas.1520335113.
- McNeill, A., Magalhaes, J., Shen, C., Chau, K.Y., Hughes, D., Mehta, A., Foltynie, T., Cooper, J.M., Abramov, A.Y., Gegg, M., Schapira, A.H., 2014. Ambroxol improves lysosomal biochemistry in glucocerebrosidase mutation-linked Parkinson disease cells. Brain 137 (Pt 5), 1481–1495. https://doi.org/10.1093/brain/awu020.
- Medina, Diego L., Fraldi, A., Bouche, V., Annunziata, F., Mansueto, G., Spampanato, C., Puri, C., Pignata, A., Martina, Jose A., Sardiello, M., Palmieri, M., Polishchuk, R., Puertollano, R., Ballabio, A., 2011. Transcriptional activation of lysosomal exocytosis promotes cellular clearance. Dev. Cell 21 (3), 421–430. https://doi.org/ 10.1016/i.devcel.2011.07.016.
- Mubariz, F., Saadin, A., Lingenfelter, N., Sarkar, C., Banerjee, A., Lipinski, M.M., Awad, O., 2023. Deregulation of mTORCI-TFEB axis in human iPSC model of GBA1associated Parkinson's disease. Front. Neurosci. 17, 1152503. https://doi.org/ 10.3389/fnins.2023.1152503.
- Murugesan, V., Chuang, W.L., Liu, J., Lischuk, A., Kacena, K., Lin, H., Pastores, G.M., Yang, R., Keutzer, J., Zhang, K., Mistry, P.K., 2016. Glucosylsphingosine is a key biomarker of Gaucher disease. Am. J. Hematol. 91 (11), 1082–1089. https://doi.org/10.1002/ajh.24491.
- Napolitano, G., Esposito, A., Choi, H., Matarese, M., Benedetti, V., Di Malta, C., Monfregola, J., Medina, D.L., Lippincott-Schwartz, J., Ballabio, A., 2018. mTOR-dependent phosphorylation controls TFEB nuclear export. Nat. Commun. 9 (1), 3312. https://doi.org/10.1038/s41467-018-05862-6.

- Neumann, J., Bras, J., Deas, E., O'Sullivan, S.S., Parkkinen, L., Lachmann, R.H., Li, A., Holton, J., Guerreiro, R., Paudel, R., Segarane, B., Singleton, A., Lees, A., Hardy, J., Houlden, H., Revesz, T., Wood, N.W., 2009. Glucocerebrosidase mutations in clinical and pathologically proven Parkinson's disease. Brain 132 (Pt 7), 1783–1794. https://doi.org/10.1093/brain/awp044.
- Osmanovic, A., Rangnau, I., Kosfeld, A., Abdulla, S., Janssen, C., Auber, B., Raab, P., Preller, M., Petri, S., Weber, R.G., 2017. FIG 4 variants in central European patients with amyotrophic lateral sclerosis: a whole-exome and targeted sequencing study. Eur. J. Hum. Genet. 25 (3), 324–331. https://doi.org/10.1038/ejhg.2016.186.
- Paciotti, S., Gatticchi, L., Beccari, T., Parnetti, L., 2019. Lysosomal enzyme activities as possible CSF biomarkers of synucleinopathies. Clin. Chim. Acta 495, 13–24. https://doi.org/10.1016/j.cca.2019.03.1627.
- Palmieri, M., Impey, S., Kang, H., di Ronza, A., Pelz, C., Sardiello, M., Ballabio, A., 2011. Characterization of the CLEAR network reveals an integrated control of cellular clearance pathways. Hum. Mol. Genet. 20 (19), 3852–3866. https://doi.org/ 10.1093/hmg/ddr306.
- Palmieri, M., Pal, R., Sardiello, M., 2017. AKT modulates the autophagy-lysosome pathway via TFEB. Cell Cycle 16 (13), 1237–1238. https://doi.org/10.1080/ 15384101.2017.1337968.
- Pringsheim, T., Jette, N., Frolkis, A., Steeves, T.D., 2014. The prevalence of Parkinson's disease: a systematic review and meta-analysis. Mov. Disord. 29 (13), 1583–1590. https://doi.org/10.1002/mds.25945.
- Rivero-Rios, P., Weisman, L.S., 2022. Roles of PIKfyve in multiple cellular pathways. Curr. Opin. Cell Biol. 76, 102086. https://doi.org/10.1016/j.ceb.2022.102086.
- Robak, L.A., Jansen, I.E., van Rooij, J., Uitterlinden, A.G., Kraaij, R., Jankovic, J., International Parkinson's Disease Genomics, C, Heutink, P., Shulman, J.M., 2017. Excessive burden of lysosomal storage disorder gene variants in Parkinson's disease. Brain 140 (12), 3191–3203. https://doi.org/10.1093/brain/awx285.
- Sardiello, M., Palmieri, M., di Ronza, A., Medina, D.L., Valenza, M., Gennarino, V.A., Di Malta, C., Donaudy, F., Embrione, V., Polishchuk, R.S., Banfi, S., Parenti, G., Cattaneo, E., Ballabio, A., 2009. A gene network regulating lysosomal biogenesis and function. Science 325 (5939), 473–477. https://doi.org/10.1126/science.1174447.
- See, S.K., Chen, M., Bax, S., Tian, R., Woerman, A., Tse, E., Johnson, I.E., Nowotny, C., Muñoz, E.N., Sengstack, J., Southworth, D.R., Gestwicki, J.E., Leonetti, M.D., Kampmann, M., 2021. PlKfyve inhibition blocks endolysosomal escape of α-synuclein fibrils and spread of α-synuclein aggregation. bioRxiv, 2021.2001.2021.427704. https://doi.org/10.1101/2021.01.21.427704.
- Settembre, C., Di Malta, C., Polito, V.A., Arencibia, M.G., Vetrini, F., Erdin, S., Erdin, S. U., Huynh, T., Medina, D., Colella, P., Sardiello, M., Rubinsztein, D.C., Ballabio, A., 2011. TFEB links autophagy to lysosomal biogenesis. Science 332 (6036), 1429–1433. https://doi.org/10.1126/science.1204592.
- Shahmoradian, S.H., Lewis, A.J., Genoud, C., Hench, J., Moors, T.E., Navarro, P.P., Castano-Diez, D., Schweighauser, G., Graff-Meyer, A., Goldie, K.N., Sutterlin, R., Huisman, E., Ingrassia, A., Gier, Y., Rozemuller, A.J.M., Wang, J., Paepe, A., Erny, J., Staempfli, A., Lauer, M.E., 2019. Lewy pathology in Parkinson's disease consists of crowded organelles and lipid membranes. Nat. Neurosci. 22 (7), 1099–1109. https://doi.org/10.1038/s41593-019-0423-2.
- Shipley, M.M., Mangold, C.A., Szpara, M.L., 2016. Differentiation of the SH-SY5Y human neuroblastoma cell line. J. Vis. Exp. 108, 53193. https://doi.org/10.3791/53193.

- Sidransky, E., Nalls, M.A., Aasly, J.O., Aharon-Peretz, J., Annesi, G., Barbosa, E.R., Bar-Shira, A., Berg, D., Bras, J., Brice, A., Chen, C.M., Clark, L.N., Condroyer, C., De Marco, E.V., Durr, A., Eblan, M.J., Fahn, S., Farrer, M.J., Fung, H.C., Ziegler, S.G., 2009. Multicenter analysis of glucocerebrosidase mutations in Parkinson's disease. N. Engl. J. Med. 361 (17), 1651–1661. https://doi.org/10.1056/NEJMoa0901281.
- Spillantini, M.G., Schmidt, M.L., Lee, V.M., Trojanowski, J.Q., Jakes, R., Goedert, M., 1997. Alpha-synuclein in Lewy bodies. Nature 388 (6645), 839–840. https://doi. org/10.1038/42166.
- Spillantini, M.G., Crowther, R.A., Jakes, R., Hasegawa, M., Goedert, M., 1998. Alpha-Synuclein in filamentous inclusions of Lewy bodies from Parkinson's disease and dementia with lewy bodies. Proc. Natl. Acad. Sci. U. S. A. 95 (11), 6469–6473. https://doi.org/10.1073/pnas.95.11.6469.
- Stojkovska, I., Wani, W.Y., Zunke, F., Belur, N.R., Pavlenko, E.A., Mwenda, N., Sharma, K., Francelle, L., Mazzulli, J.R., 2022. Rescue of alpha-synuclein aggregation in Parkinson's patient neurons by synergistic enhancement of ER proteostasis and protein trafficking. Neuron 110 (3), 436–451 e411. https://doi.org/10.1016/j.neuron.2021.10.032.
- Sun, Y., Hou, S., Zhao, K., Long, H., Liu, Z., Gao, J., Zhang, Y., Su, X.D., Li, D., Liu, C., 2020. Cryo-EM structure of full-length alpha-synuclein amyloid fibril with Parkinson's disease familial A53T mutation. Cell Res. 30 (4), 360–362. https://doi.org/10.1038/s41422-020-0299-4.
- Uras, G., Li, X., Manca, A., Pantaleo, A., Bo, M., Xu, J., Allen, S., Zhu, Z., 2022. Development of p-tau differentiated cell model of Alzheimer's disease to screen novel acetylcholinesterase inhibitors. Int. J. Mol. Sci. 23 (23), 14794. htt ps://www.mdpi.com/1422-0067/23/23/14794.
- Vieira, S.R.L., Mezabrovschi, R., Toffoli, M., Del Pozo, S.L., Menozzi, E., Mullin, S., Yalkic, S., Limbachiya, N., Koletsi, S., Loefflad, N., Lopez, G.J., Gan-Or, Z., Alcalay, R.N., Sidransky, E., Schapira, A.H.V., 2024. Consensus guidance for genetic counseling in GBA1 variants: a focus on Parkinson's disease. Mov. Disord. https://doi.org/10.1002/mds.30006.
- Wallings, R.L., Humble, S.W., Ward, M.E., Wade-Martins, R., 2019. Lysosomal dysfunction at the centre of Parkinson's disease and frontotemporal dementia/ amyotrophic lateral sclerosis. Trends Neurosci. 42 (12), 899–912. https://doi.org/ 10.1016/j.tins.2019.10.002.
- Xicoy, H., Wieringa, B., Martens, G.J., 2017. The SH-SY5Y cell line in Parkinson's disease research: a systematic review. Mol. Neurodegener. 12 (1), 10. https://doi.org/ 10.1186/s13024-017-0149-0.
- Yang, S.Y., Beavan, M., Chau, K.Y., Taanman, J.W., Schapira, A.H.V., 2017. A human neural crest stem cell-derived dopaminergic neuronal model recapitulates biochemical abnormalities in GBA1 mutation carriers. Stem Cell Reports 8 (3), 728–742. https://doi.org/10.1016/j.stemcr.2017.01.011.
- Yang, S.Y., Taanman, J.W., Gegg, M., Schapira, A.H.V., 2022. Ambroxol reverses tau and alpha-synuclein accumulation in a cholinergic N370S GBA1 mutation model. Hum. Mol. Genet. 31 (14), 2396–2405. https://doi.org/10.1093/hmg/ddac038.
- Zhang, S., Zhu, R., Pan, B., Xu, H., Olufemi, M.F., Gathagan, R.J., Li, Y., Zhang, L., Zhang, J., Xiang, W., Kagan, E.M., Cao, X., Yuan, C., Kim, S.J., Williams, C.K., Magaki, S., Vinters, H.V., Lashuel, H.A., Garcia, B.A., Peng, C., 2023. Post-translational modifications of soluble alpha-synuclein regulate the amplification of pathological alpha-synuclein. Nat. Neurosci. 26 (2), 213–225. https://doi.org/10.1038/s41593-022-01239-7.